Practical Residual Error of Interference Cancellation for Spread MSK with a Pseudo-noise Preamble

Qiongjie Lin, Jinsu Lee, and Mary Ann Weitnauer
School of Electrical and Computer Engineering
Georgia Institute of Technology, Atlanta, Georgia 30332-0250
Email: lin3@gatech.edu; jlee973@gatech.edu; maweit@gatech.edu

***Abstract*—Interference cancellation (IC) has been proposed to improve bandwidth utilization for the majority of modern wireless networks. We claim that the conventional model for IC residual error, which is that the residual error power is simply a fraction of the power of the packet being cancelled, is overly simplified. In this paper, we evaluate the practical residual error of IC with spread MSK modulation in a flat fading environment for a low power wide area (LPWA) wireless sensor network application. In particular, we address the two-packets-overlapping scenario as a function of the signal to noise ratio (SNR) of each packet and the overlapping degree. Using software-defined radios, we demonstrate that the average realistic residual error power based on packet transmission with a single pseudo-noise preamble is not a constant fraction of the power of the packet being canceled. Rather, it depends on the synchronization and channel estimation errors, which in turn, depend on the SINR of the stronger packet preamble.**

***Index Terms*—Interference cancellation, wireless sensor network, synchronization error, software-defined radio**

I. Introduction

Though interference cancellation (IC) dates back to the 1990s [1], [2], [3] there has been a surge of recent interest in analyzing ALOHA-based network protocols that do IC [4]–[10]. IC is attractive because it allows multiple co-channel packets occurring at the same time to be decoded by a single-antenna receiver, resulting in significantly improved reliability and throughput. In IC, the effects of a decoded strong packet are subtracted from stored samples of the received signal, thereby making possible the capture of weaker packets. Successive interference cancellation (SIC) is the repeated application of IC [11], [12]. In these recent analyses, the authors either ignore the interference caused by the residual error of imperfect cancellation [7], [8] or they model the power of the residual error very simply as a fixed percentage of the power of the packet being canceled [6], [9], [10]. We refer to the latter case as the conventional model.

In this paper, we theoretically and experimentally investigate the characteristics of the residual error for unsynchronized packets modulated with minimum shift keying (MSK) and that begin with a pseudo-noise preamble, followed by a spread MSK payload. This signal design is appropriate for some Internet of Things (IoT) applications in unlicensed bands, including severely power constrained transmit-only and beaconing devices [13]–[16]. We show that the characteristics of practical residual errors deviate significantly from the simple model.

IC has been shown to improve bandwidth utilization in cellular networks [17], which have centralized control and synchronized clocks among wireless devices, and where the towers determine the best transmit power, coding rate and/or spreading codes to enable the disambiguation of different uplink transmissions. However, in the networks we are considering, there is no centralized control over power, no time and frequency synchronization between wireless devices, and in general the techniques to facilitate the disambiguation at transmitter side are constrained by the physical limitations of wireless sensors.

Several recent reports of IC experiments exist [18]–[20], including for Zigbee networks [21]. In [20], SIC with carrier sense threshold is adapted to work in uncontrolled network scenarios for the IEEE 802.15.4 (ZigBee). However, all these studies focus on the packet delivery rate improvement of SIC in WLANs, by handling the hidden terminals problem. These studies do not focus on characterizing the residual error.

The rest of the paper is organized as follows. Section II describes the system model considered for this work. Section III describes our experiment design. In Section IV, we present our experiment results obtained using a software-defined radio platform. Section V concludes the paper.

II. System Model

We study the uplink of the random access wireless network illustrated in Fig.1. The system is composed of many randomly distributed low power transmitters and a single-antenna gateway (GW). We assume that the GW always stores the latest K samples it received, where K is at least large enough to include a packet and the processing time to decode and cancel a packet. With IC, when a packet has been decoded by the GW, the packet's physical layer samples are synthesized or regenerated and subtracted from the stored samples.

In our physical layer model, each packet is composed of only two parts: a known preamble and a payload of random data. Following a conventional direct sequence spread spectrum (DSSS) approach [22], the payload is composed of L_2 bits, which are spread by a DSSS code with spreading factor C, so that the total number of chips or MSK symbols in the payload is $L_2 \cdot C$. We adopt the practical synchronization scheme proposed in [23]. The preamble is modulated using just one PN sequence, C_p symbols long, using MSK, such that each MSK symbol in the preamble is the same length in

978-1-5090-1328-9/16/$31.00 ©2016 IEEE

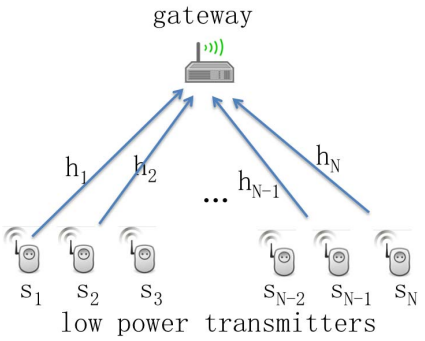

Fig. 1. Illustration of the network architecture.

time as a chip in the payload. The preamble is not constructed by spreading bits, however, it is convenient to define a variable $L_1 = \frac{C_p}{C}$, which would be the number of bits in the preamble if we constructed the preamble by spreading bits.

When considering MSK, a binary continuous phase modulation (CPM), the complex baseband signal from a transmitter can be expressed as

$$x(t) = \sqrt{\frac{2E_c}{T_c}} exp\{j\phi(t;\chi)\}, \tag{1}$$

where E_c is the energy per transmitted chip with duration T_c. $\phi(t;\chi)$ is the phase of the signal, which is represented as

$$\phi(t;\alpha) = 2\pi d \sum_{i=0}^{C_s-1} \chi_i q(t - iT_c), \tag{2}$$

where χ_i is a sequence $\{\chi_0, \chi_1, \ldots, \chi_{C_s-1}\}$ of chips such that $\chi_i \in \{\pm 1\}$. C_s is the total number of such chips for one packet, so that $C_s = C_p + L_2 * C = (L_1 + L_2) * C$. The variable d is the modulation index of CPM, and $d = \frac{1}{2}$ for MSK. The waveform $q(t)$ is the phase response of MSK.

We assume the flat fading channel is modeled as $h = \gamma e^{j\theta}$, where γ is the magnitude and θ is the phase. The complex baseband representation of the received signal is

$$y(t) = e^{j(2\pi f_d t)} hx(t - \tau) + z(t), \tag{3}$$

where f_d is the frequency offset, τ is the timing offset, and $z(t)$ is complex baseband AWGN with zero mean and power spectral density N_0. In practice, $y(t)$ is sampled N times per chip symbol with sampling rate of f_s. This results in a discrete-time version of of received signal as

$$y[i] = y(\frac{iT_c}{N}) = e^{j(2\pi\omega i)} hx[i] + z[i], \tag{4}$$

where $\omega = f_d T_c / N$ is the normalized frequency offset with respect to the sampling frequency. $x[i] = x(\frac{iT_c}{N} - \tau)$ and $z[i]$ are the sampled versions of $x(t - \tau)$ and $z(t)$, respectively.

A. Instantaneous Residual Error

In practical IC, the subtraction of the decoded packet is not perfect due to the imperfect synchronization and channel estimation. An interference-insensitive timing synchronization approach is available [23], therefore we assume the timing synchronization is perfect. Let ω, $\hat{\omega}$ be the real and estimated normalized carrier frequency offset (CFO), respectively, between TX and GW. $\hat{h} = \hat{\gamma} e^{j\hat{\theta}}$ is the estimated channel. The residual IC error at sample index i for the successfully decoded packet $y[i]$ after subtracting the reconstructed signal $\hat{y}[i]$ is

$$\begin{aligned} e[i] &= e^{j(2\pi\omega i)} hx[i] - e^{j(2\pi\hat{\omega} i)} \hat{h} x[i] \\ &= x[i] \Big(\gamma e^{j(2\pi\omega i + \theta)} - \hat{\gamma} e^{j(2\pi\hat{\omega} i + \hat{\theta})} \Big). \end{aligned} \tag{5}$$

Let $\beta_i = 2\pi\omega i + \theta, \hat{\beta}_i = 2\pi\hat{\omega} i + \hat{\theta}$, and $\Delta\beta_i = \beta_i - \hat{\beta}_i$. Then the magnitude squared of the residual error is

$$\begin{aligned} |e[i]|^2 &= e[i] e^*[i] \\ &= |x[i]|^2 \Big(\gamma^2 + \hat{\gamma}^2 - \gamma\hat{\gamma} e^{j\Delta\beta_i} - \hat{\gamma}\gamma e^{-j\Delta\beta_i} \Big) \\ &= |x[i]|^2 \Big(\gamma^2 + \hat{\gamma}^2 - 2\gamma\hat{\gamma} cos(\Delta\beta_i) \Big). \end{aligned} \tag{6}$$

Define the estimation errors in the channel and CFO as $e_\gamma = \gamma - \hat{\gamma}, e_\theta = \theta - \hat{\theta}, e_\omega = \omega - \hat{\omega}$, respectively. The expectation of instantaneous residual error after cancellation becomes

$$E\{|e[i]|^2\} = \sigma_S^2 E\Big\{ \gamma^2 + \hat{\gamma}^2 - 2\gamma\hat{\gamma} cos(2\pi e_\omega i + e_\theta) \Big\}, \tag{7}$$

where σ_S^2 is the average transmitted signal power. According to Eq.(7), the instantaneous residual error is not constant over the packet, but is a function of time determined by the residual errors of channel gain, frequency and phase estimations. For larger sample index i, the residual error tends to be larger due to the larger accumulated phase offset $\Delta\beta_i = 2\pi e_\omega i + e_\theta$.

B. Residual Error to Signal Ratio (ESR)

To characterize the practical residual error for the overlapping scenario, we propose the residual error to signal ratio (ESR) metric, which is the average power of residual error in overlapping period, normalized by the average power of the stronger packet over the same overlapping interval, as

$$ESR = \frac{\frac{1}{N_{OL}} \sum_{i=I_s^s}^{I_e^s} |e_s[i]|^2}{\frac{1}{N_{OL}} \sum_{i=I_s^s}^{I_e^s} |y_s[i]|^2}, \tag{8}$$

where I_s^s is the starting sampling index of the overlapped portion of the stronger packet, and I_e^s is the ending sampling index of the portion.

By substituting the instantaneous residual error from Eq.(7), the ESR can be written as

$$\begin{aligned} ESR &= \frac{\sigma_S^2 |\gamma^s|^2}{\sigma_S^2 |\gamma^s|^2 + \sigma_N^2} + \frac{\sigma_S^2 |\hat{\gamma^s}|^2}{\sigma_S^2 |\gamma^s|^2 + \sigma_N^2} \\ &- \frac{2\sigma_S^2 \gamma^s \hat{\gamma^s} \sum_{i=I_i^s}^{I_e^s} cos(2\pi e_\omega i + e_\theta)}{(\sigma_S^2 |\gamma^s|^2 + \sigma_N^2) N_I} \\ &= \frac{SNR^s}{SNR^s + 1} + \frac{\widehat{SNR^s}}{SNR^s + 1} \\ &- \frac{2\widehat{SNR^s}}{SNR^s + 1} * \frac{\sum_{i=I_s^s}^{I_e^s} cos(2\pi e_\omega i + e_\theta)}{N_I}, \end{aligned} \tag{9}$$

where $SNR^s = \frac{|\gamma^s|^2 \sigma_S^2}{\sigma_N^2}$, $\widehat{SNR^s} = \frac{|\hat{\gamma^s}|^2 \sigma_S^2}{\sigma_N^2}$, and $\widehat{SNR^s} = \frac{\gamma^s \hat{\gamma^s} \sigma_S^2}{\sigma_N^2}$ are the real and reconstructed SNRs of the strong packet.

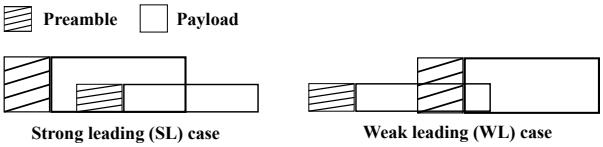

Fig. 2. Illustration of overlapping scenarios

Define the overlapping degree $O = \frac{N_I}{N_p}$, where $N_I = I_e^s - I_s^s + 1$ is the number of overlapping samples, and $N_p = (L_1 + L_2) * C * N$ is the total number samples per packet. By applying the Lemma: $\sum_{k=0}^{n} cos(ak + z) = csc(\frac{a}{2}) sin(\frac{1}{2}a(n+1)) cos(\frac{an}{2} + z)$ [24] into Eq.(9), the ESR then becomes:

$$ESR = \frac{SNR^s}{SNR^s + 1} + \frac{\overline{SNR^s}}{SNR^s + 1} - \frac{2\widehat{SNR^s}}{SNR^s + 1} * K(e_\omega^s, e_\theta^s, I_s^s, I_e^s), \tag{10}$$

where

$$K(e_\omega^s, e_\theta^s, I_s^s, I_e^s) = \underbrace{\frac{sin(\pi e_\omega^s O N_p)}{sin(\pi e_\omega^s) O N_p}}_{C_1} * \underbrace{cos(\pi e_\omega^s (I_e^s + I_s^s) + \pi e_\omega^s + e_\theta^s)}_{C_2} \tag{11}$$

As we can see in Eqs.(10) and (11), the ESR is determined by the SNR of the strong packet, frequency and phase synchronization errors e_ω^s, e_θ^s, the overlapping degree, O, and the location of the interference in terms of the start and end points of the interference, I_s^s, I_e^s.

According to Eq.(11), the key term K is composed of two parts: C_1, C_2, where $C_1(e_{\omega,O}^s)$ is a function of frequency synchronization error and overlapping degree, while $C_2(e_\omega^s, e_\theta^s, I_e^s, I_s^s)$is a function of synchronization error as well as the location of the interference.

We consider two types of overlapping scenarios as illustrated in Fig.2: the strong leading (SL) case and the weak leading (WL) case. For the SL case, the end of the strong packet is overlapped with the beginning of the weak packet, while the weak packet is leading the interference part for WL case. For the SL case, $I_e^s = N_p$ is fixed, and $I_s^s = I_e^s - ON_p = N_p(1 - O)$, while for WL case, $I_s^s = 1$ is fixed, and $I_e^s = I_s^s + ON_p = N_pO + 1$.

Therefore, the subterm C_2 in Eq. (11) is different for SL and WL cases, which are

$$C_2^{SL} = cos\Big(- \pi e_\omega^s N_p O + 2\pi e_\omega^s N_p + \pi e_\omega^s + e_\theta^s \Big), \tag{12}$$

$$C_2^{WL} = cos\Big(\pi e_\omega^s N_p O + 3\pi e_\omega^s + e_\theta^s \Big). \tag{13}$$

In the next section, we see how experimental data validate Eqs. (6), (12), and (13) in particular.

III. Experiment Design

In this section, we design and conduct a large number of experiments to measure the defined metric ESR, based on the successful decoding sets with BER of zero. We employ three

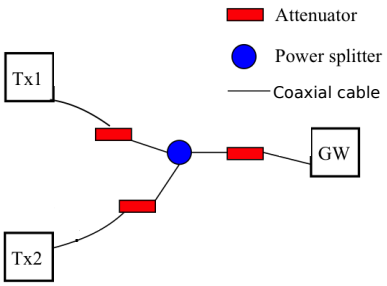

(a) The diagram of experiment setup.

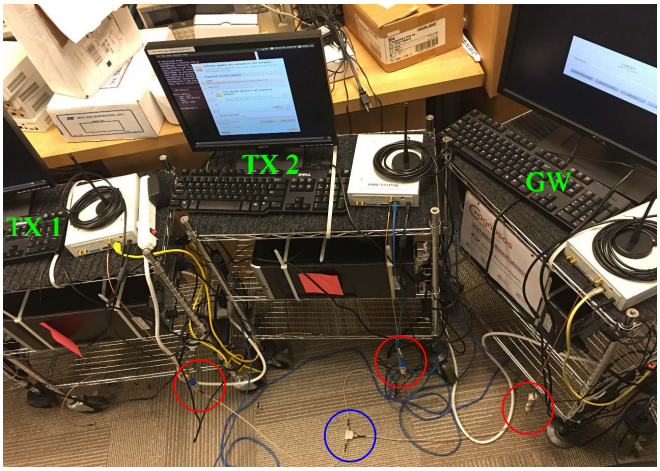

(b) The photo of experiment setup

Fig. 3. Experiment setup. (antenna was disabled for the experiments; red circle: attenuator; blue circle: splitter.)

software defined radios (SDRs), as shown in Fig.3, to conduct the experiment. Two of them are the transmitters, and the other one is a GW. They are connected through cable, power splitter, and attenuators to avoid the effect of unstable channel.

According to the theoretical analysis in Eq.(7), we know the practical residual error is determined by synchronization performance, channel estimation performance, as well as signal and noise powers. Therefore, we design the experiment in terms of a set, as illustrated in Fig.4, to evaluate the residual error in terms of SNR, signal to interference and noise ratio (SINR), and random overlapping scenario. As shown in Fig.4(a), the two TXs are scheduled to transmit packets continuously at different repetition rates once activated at time $t_{0,1}$ and $t_{0,2}$, respectively. By controlling the delay between the start times $t_\Delta = |t_{0,1} - t_{0,2}|$, we are able to create different overlapping degree situations. When Tx1 with repetition rate $R_1 = \frac{1}{3}$ transmits at lower power, and TX2 with repetition rate $R_2 = \frac{1}{5}$ transmits at higher power, the designed received signal at GW is illustrated as Fig.4(b), which has a repetition pattern as well. Each set contains both overlapping cases SL and WL, for a particular overlapping degree, O. We also have one interference-free reference of the strong packet and three interference-free references of the weak packet for each set.

In the experiment, we do not have access to instananeous residual error $e_s[i]$. Instead, we measure random outcomes of

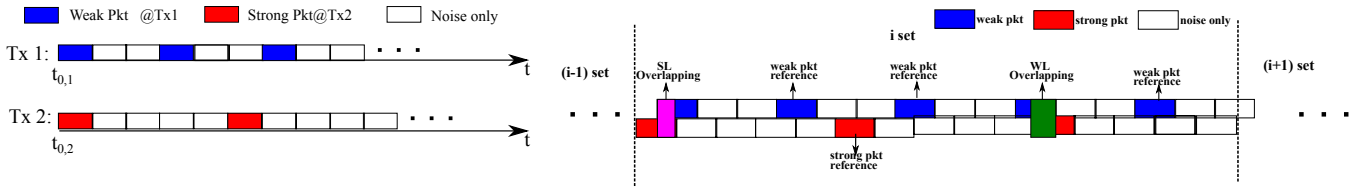

(a) Packet transmission schedule

(b) One set of overlapping degrees

Fig. 4. Illustration of experiment design

ESR, approximated as

$$ESR = \frac{|E\{|\hat{y}_w|^2\} - E\{|y_w|^2\}|}{E\{|\hat{y}_s|^2|}, \tag{14}$$

where $\hat{y}_w$ is a weak packet with residual error after subtracting of strong packet and y_w is an interference-free weak packet, and $\hat{y}_s$ is the overlapping part of an interference-free strong packet.

For the experiment, we use a payload length of 48 information bits and a basic preamble length of 16 information bits. The other system parameters for the experiments are listed in the table below.

TABLE I
PARAMETER OPTIMIZATION

Carrier frequency	430MHz
Sampling rate	$F_s = 200KHz$
Samples per chip	$N = 32$
Spreading factor	$C = 15$
Modulation	MSK
Preamble ratio	$\epsilon = 0.25$
Packet length	$L = 64$

We transmit large numbers of sets at different transmitter power levels, overlapping degrees, and spreading factors. We calculate the average residual error factor ESR based only on the successfully decoded sets with BER of zero. Each average is based on 200 sets.

A. Experiment data

Fig.5(a) shows the experimentally received signals, which match the set definition in Fig.4(b). The corresponding packet detection metric is shown in Fig.5(b) with the peaks indicating the starts of packets (SOPs). The peaks for the strong packets are higher than for the weak packets. The red double-ended arrows in Fig.5(b) indicate the difference between the peak of the metric and the "noise" level near the peak; this difference is proportional to the SINR of the preamble. Thus Fig.5(b) reflects that the preamble for the second weak packet, which is an interference-free reference, has a higher SINR than the preamble of the first weak packet, which has interference.

According to the measurements after IC processing in Figs.5(c) and 5(d), we find the instantaneous residual error is not constant over the packet but tends to initially worsen over time in Fig.5(c) as we expected based on Eq.(7). The error is small at the beginning because the channel estimate based on the preamble compensates for the initial phase offset. As we can see in Fig.5(d), we only see clear peaks indicating the SOPs of weak packets, which demonstrates the effectiveness

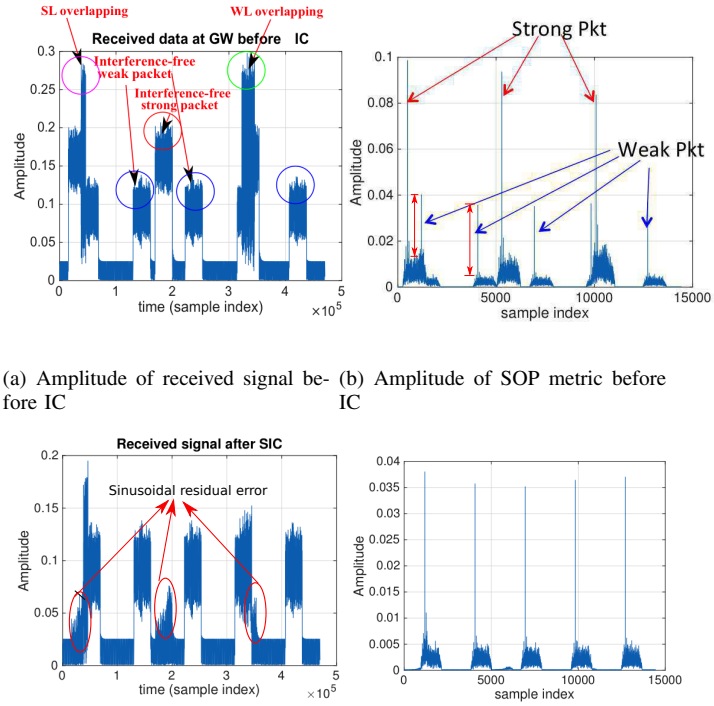

(a) Amplitude of received signal before IC

(b) Amplitude of SOP metric before IC

(c) Amplitude of received signal after IC

(d) Amplitude of SOP metric after IC

Fig. 5. The received signal at GW for IC processing.

of the cancellation and ability of the preamble correlation inherent in SOP estimation to suppress the interference from the residual error. Meanwhile, the weak packets are decoded without error after IC.

IV. Experimental Results

According the the theretical model in Eq.(10) and (11), we expect to see that the practical residual error is affected by the SNR of the strong packet and the synchronization errors, which are highly determined by the SINR on the preamble of the strong packet. Therefore, in this section, we conduct experiments to demonstrate the effects of SNR and SINR by controlling the TX powers of the overlapping packets.

A. Experiment Measurement: TX power effects

Let $P^s(P^w)$ be the power of the strong (weak) packet, in dBm. For the results in this subsection, we fix the TX power difference, $P_\Delta = P^s - P^w = 7$dBm, and spreading factor

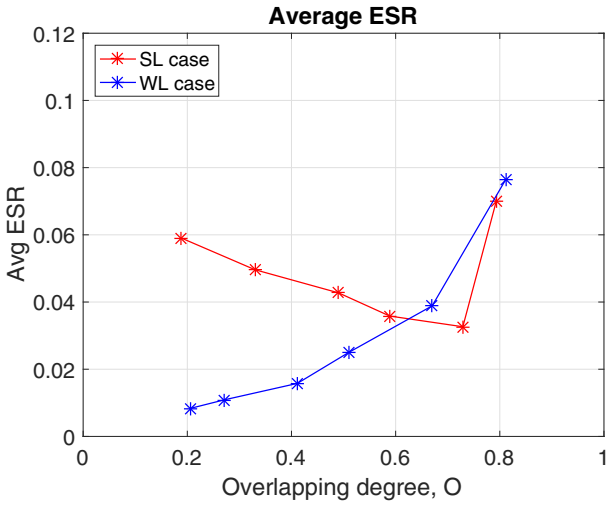

Fig. 6. Experiment result with $SNR^s = 18.96dB, SNR^w = 12.20dB$, $SINR^s = 6.50dB$.

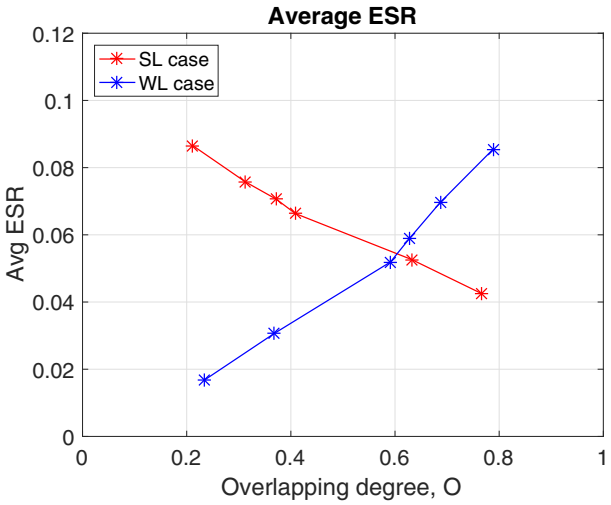

Fig. 7. Experiment result with $SNR^s = 11.98dB, SNR^w = 5.18dB, SINR^s = 5.65dB$.

$C = 15$, and measure the corresponding averaged ESR over 200 sets in terms of different TX power levels, to evaluate the residual error performance in terms of SNR.

1) High TX power: we first conduct the experiments at high power levels with $P^s = 0dBm$ and $P^w = -7dBm$. The corresponding residual error measurements are shown in Fig.6. We observe that when the overlapping degree grows, the corresponding averaged ESR decreases for the SL case, while it increases for the WL case. Intuitively, this happens because the instantaneous error is increasing but the ESR is averaged only over the overlapping period. Thus, in the SL case, for small O, only the highest instantaneous error is captured in the average. On the other hand, in the WL case, for small O, only the lowest instantaneous errors are captured in the average. As O grows for the SL (WL) case, smaller (larger) values of the instantaneous error are averaged in, causing the downward (upward) trends in the graph. We also observe that SL ESR goes up dramatically when $O = 0.8$. This happens because the preamble accounts for a quarter of the total packet. So when $O > 0.75$, the preamble of the strong packet for the SL case is also interfered so that synchronization and channel estimation performance are sacrificed. On the other hand, when $O < 0.25$, there is interference on only part of the preamble of the strong packet for the WL case, and we should expect lower residual error.

2) Low TX power: to demonstrate the effect of the SNR, we conduct experiments at the lower TX power levels of $P^s = -7dBm$ and $P^w = -14dBm$. The corresponding residual error measurements are are shown in Fig.7. We observed that when the SNR of the strong packet reduces, the corresponding ESR increases, compared with the results in Fig.6 for the SL case, while it does not change much for WL case. This happens because the synchronization and channel estimation performances are mainly affected by the SNR for the SL case as there is no interference on the preamble, and the ESR grows as the synchronization performance gets worse with lower SNR. However for the WL case, the synchronization and channel estimation performances are mainly affected by the SINR, so the WL ESR curves are not too different in Figs 6 and 7.

B. Experiment Measurement: SINR effects

In this subsection, we evaluate the effect of SINR by reducing the TX power difference from 7dBm to 4dBm while keeping the SNR of the strong packet the same as in Fig 6, and then we measure the corresponding averaged ESR. The TX powers are $P^s = 0dBm$ and $P^w = -4dBm$ and we keep the spreading length of 15. The corresponding residual error measurements are are shown in Fig.8.

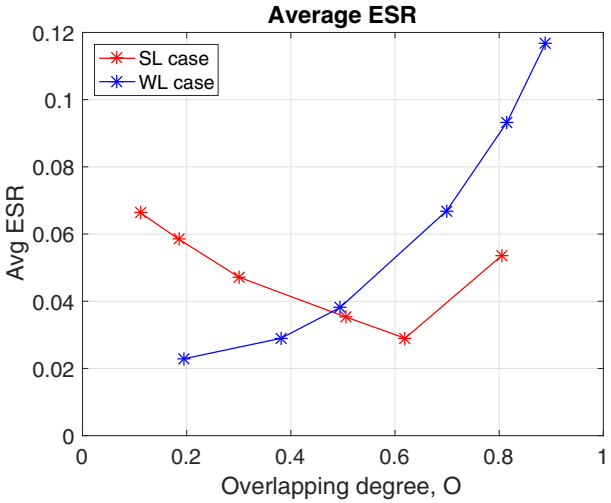

Fig. 8. Experiment result with $SNR^s = 18.89dB, SNR^w = 15.15dB, SINR^s = 3.62dB$

By comparing the results in Figs. 6 and 8, we observe that the ESR is similar for SL case, while it is worse in Fig.8 for the WL case. When the SNR does not change, the synchronization and channel estimation performances are similar for SL without interference on the preamble, but sacrificed for the WL case with interference on the preamble as SINR decreases.

While there seem to be clear trends in our data, we observe that some of the average ESR curves are not so smooth. This is likely caused by too few trials in the average. Another consideration is that we used the same payload data in all packets, which might contribute artifacts into our results. We will try to address both of these deficiencies in our future work.

V. Conclusion

In this work, we evaluate the practical residual error for continuous phase modulation through analysis and experiments on SDRs. The instantaneous residual error is demonstrated to have a sinusoidal pattern over time caused by the synchronization error. The averaged residual error is shown through theory and experiments to be a function of the overlapping degree, the SINR of the preamble, the SNR, and the length of the preamble. Thus the conventional residual error model, which assumes the residual error is independent of the level and location of the interference, is proved to be unrealistic in pratice. More theoretical analysis of the residual error with respect to various parameters will be studied in our future work.

Acknowledgment

The authors gratefully acknowledge helpful discussions with members of Cognosos Inc. and partial support of this research by the Georgia Research Alliance of the State of Georgia and from the U.S. National Science Foundation (NSF) under Grant CNS-1513884.

References

[1] M. K. Varanasi and B. Aazhang, "Multistage detection in asynchronous code-division multiple-access communications," *Communications, IEEE Transactions on*, vol. 38, no. 4, pp. 509–519, 1990.

[2] A. Duel-Hallen, "Decorrelating decision-feedback multiuser detector for synchronous code-division multiple-access channel," *Communications, IEEE Transactions on*, vol. 41, no. 2, pp. 285–290, 1993.

[3] P. Patel and J. Holtzman, "Analysis of a simple successive interference cancellation scheme in a DS/CDMA system," *Selected Areas in Communications, IEEE Journal on*, vol. 12, no. 5, pp. 796–807, 1994.

[4] E. Casini, R. De Gaudenzi, and O. R. Herrero, "Contention resolution diversity slotted ALOHA (CRDSA): An enhanced random access schemefor satellite access packet networks," *Wireless Communications, IEEE Transactions on*, vol. 6, no. 4, pp. 1408–1419, 2007.

[5] G. Liva, "Graph-based analysis and optimization of contention resolution diversity slotted ALOHA," *Communications, IEEE Transactions on*, vol. 59, no. 2, pp. 477–487, 2011.

[6] A. Zanella and M. Zorzi, "Theoretical analysis of the capture probability in wireless systems with multiple packet reception capabilities," *Communications, IEEE Transactions on*, vol. 60, no. 4, pp. 1058–1071, 2012.

[7] C. Stefanovic, P. Popovski, and D. Vukobratovic, "Frameless aloha protocol for wireless networks," *IEEE Communications Letters*, vol. 16, no. 12, pp. 2087–2090, 2012.

[8] O. del Rio Herrero and R. De Gaudenzi, "Generalized analytical framework for the performance assessment of slotted random access protocols," *Wireless Communications, IEEE Transactions on*, vol. 13, no. 2, pp. 809–821, 2014.

[9] A. Zanella, A. Biral, and M. Zorzi, "Asymptotic throughput analysis of massive m2m access," in *Information Theory and Applications Workshop (ITA), 2015*. IEEE, 2015, pp. 64–69.

[10] M. A. Weitnauer, Q. Lin, H. Zhang, H. Tian, S. M. Nowlan, G. Nyengele, S. Mohan, and J. Stratigos, "Reliability and longer range for low power transmitters with on demand network MIMO," in *2016 IEEE International Conference on RFID (RFID) (IEEE RFID 2016)*, Orlando, USA, May 2016.

[11] A. Duel-Hallen, "Decorrelating decision-feedback multiuser detector for synchronous code-division multiple-access channel," *Communications, IEEE Transactions on*, vol. 41, no. 2, pp. 285–290, 1993.

[12] A. Zanella and M. Zorzi, "Theoretical analysis of the capture probability in wireless systems with multiple packet reception capabilities," *Communications, IEEE Transactions on*, vol. 60, no. 4, pp. 1058–1071, 2012.

[13] C. Huebner, R. Cardell-Oliver, S. Hanelt, T. Wagenknecht, and A. Monsalve, "Long-range wireless sensor networks with transmit-only nodes and software-defined receivers," *Wireless Communications and Mobile Computing*, vol. 13, no. 17, pp. 1499–1510, 2013.

[14] T. R. Park and M. J. Lee, "Power saving algorithms for wireless sensor networks on ieee 802.15. 4," *Communications Magazine, IEEE*, vol. 46, no. 6, pp. 148–155, 2008.

[15] P. Parsch, A. Masrur, and W. Hardt, "Designing reliable home-automation networks based on unidirectional nodes," in *Industrial Embedded Systems (SIES), 2014 9th IEEE International Symposium on*. IEEE, 2014, pp. 88–95.

[16] B. Firner, "Transmit only for dense wireless networks," Ph.D. dissertation, Rutgers University-Graduate School-New Brunswick, 2014.

[17] J. G. Andrews, "Interference cancellation for cellular systems: a contemporary overview," *Wireless Communications, IEEE*, vol. 12, no. 2, pp. 19–29, 2005.

[18] Y. Yan, P. Yang, X.-Y. Li, Y. Zhang, J. Lu, L. You, J. Wang, J. Han, and Y. Xiong, "Wizbee: Wise zigbee coexistence via interference cancellation with single antenna," *Mobile Computing, IEEE Transactions on*, vol. 14, no. 12, pp. 2590–2603, 2015.

[19] M. Grieger, P. Marsch, and G. Fettweis, "Uplink base station cooperation by iterative distributed interference subtraction," in *Personal, Indoor and Mobile Radio Communications, 2009 IEEE 20th International Symposium on*. IEEE, 2009, pp. 1973–1977.

[20] D. Halperin, T. Anderson, and D. Wetherall, "Taking the sting out of carrier sense: interference cancellation for wireless lans," in *Proceedings of the 14th ACM international conference on Mobile computing and networking*. ACM, 2008, pp. 339–350.

[21] L. Kong and X. Liu, "mZig: Enabling multi-packet reception in zigbee," in *Proceedings of the 21st Annual International Conference on Mobile Computing and Networking*. ACM, 2015, pp. 552–565.

[22] R. C. Dixon, *Spread Spectrum Systems with Commercial Applications*. John Wiley & Sons, Inc., 1994.

[23] Q. Lin and M. A. Weitnauer, "Interference-insensitive synchronization scheme of MSK for transmit-only wireless sensor networks," in *ICC'16-Wireless Communications Symposium, IEEE International Conference on Communications*, 2016.

[24] A. Zygmund, *Trigonometric Series*. Cambridge University Press, 2002, vol. 1.